Surface Science 653 (2016) 153–162

Contents lists available at ScienceDirect

Surface Science

journal homepage: www.elsevier.com/locate/susc

Density functional theory study of the interaction of H_2O, CO_2 and CO with the ZrO_2 (111), Ni/ZrO_2 (111), YSZ (111) and Ni/YSZ (111) surfaces

Abdelaziz Cadi-Essadek [a], Alberto Roldan [b], Nora H. de Leeuw [a,b,*]

[a] Department of Chemistry, University College London, 20 Gordon Street, London WC1H 0AJ, United Kingdom
[b] School of Chemistry, Cardiff University, Main Building, Park Place, CF10 3AT Cardiff, United Kingdom

ARTICLE INFO

Article history:
Received 2 March 2016
Received in revised form 18 June 2016
Accepted 21 June 2016
Available online 23 June 2016

Keywords:
Triple phase boundary
Yttria-stabilized zirconia
Molecule-surface interaction
Fuel cell
Supported nanoparticles
Surface science

ABSTRACT

The triple phase boundary (TPB), where the gas phase, Ni particles and the yttria-stabilised zirconia (YSZ) surface meet, plays a significant role in the performance of solid oxide fuel cells (SOFC). Indeed, the key reactions take place at the TPB, where molecules such as H_2O, CO_2 and CO interact and react. We have systematically studied the interaction of H_2O, CO_2 and CO with the dominant surfaces of four materials that are relevant to SOFC, i.e. ZrO_2(111), Ni/ZrO_2(111), YSZ(111) and Ni/YSZ(111) of cubic ZrO_2 stabilized with 9% of yttria (Y_2O_3). The study employed spin polarized density functional theory (DFT), taking into account the long-range dispersion forces. We have investigated up to five initial adsorption sites for the three molecules and have identified the geometries and electronic structures of the most stable adsorption configurations. We have also analysed the vibrational modes of the three molecules in the gas phase and compared them with the adsorbed molecules. A decrease of the wavenumbers of the vibrational modes for the three adsorbed molecules was observed, confirming the influence of the surface on the molecules' intra-molecular bonds. These results are in line with the important role of Ni in this system, in particular for the CO adsorption and activation.

1. Introduction

The solid oxide fuel cell (SOFC) is an electrochemical device that converts electricity by oxidizing fuel, e.g. hydrogen, through an environmentally sustainable process [1]. A common anode used for this device is yttria-stabilized zirconia (YSZ) with supported Ni particles. The main advantages of the Ni/YSZ cermet (ceramic matrix (YSZ) bonded to metal particles (Ni)) [2] over other materials are, for instance, its good thermal expansion, ionic conductivity, high catalytic activity, mechanical/chemical stability and compatibility with the electrolyte [3,4]. Several experimental and theoretical studies of the Ni/YSZ cermet have endeavoured to gain understanding of the microstructure of this material, since the material's atomic level structure and processes lie at the core of the performance of the SOFC anode [5].

One of the species used as fuel in the SOFC are H_2 and CO which are oxidized at the anode of the SOFC [6]. Electrochemical oxidation of H_2 is a multistep process where adsorption, surface reactions and charge transfer are observed during the reaction [7]. The reaction at the anode is described by reaction (R.1) [8]:

$$H_2 + O^{2-} \rightleftharpoons H_2O + 2e^- \quad (R.1)$$

In the CO oxidation on Ni/YSZ, CO adsorbs associatively on Ni and then diffuses towards the triple phase boundary (TPB), where the gas phase, Ni particles and YSZ surface meet. Here, it is oxidized by O^{2-} coming from the electrolyte i.e. the solid oxide (reaction (R.2)) [9].

$$CO + O^{2-} \rightleftharpoons CO_2 + 2e^- \quad (R.2)$$

Instead of pure H_2 or CO, H_2/CO mixtures can be used leading to more complicated mechanisms since other reactions than direct oxidations are involved such as water-gas shifting [6] (reaction (R.3)) [10–12].

$$CO + H_2O \rightleftharpoons CO_2 + H_2 \quad (R.3)$$

All these molecules interact with the supported Ni and the surface, thus necessitating the study of these molecules in contact with the

* Corresponding author at: Department of Chemistry, University College London, 20 Gordon Street, London WC1H 0AJ, United Kingdom.
E-mail address: DeLeeuwN@cardiff.ac.uk (N.H. de Leeuw).

http://dx.doi.org/10.1016/j.susc.2016.06.008

TPB, which plays a key role in the performance of the SOFC [13]. In the past few years many researchers have investigated the microstructure and the chemistry of the TPB. For example, Liu et al. [14] have shown experimentally that impurities such as SiO_2 can degrade the Ni/YSZ grain boundaries, whereas Jensen et al. [15] have shown that impurities segregate from the bulk of the YSZ material and accumulate along the TPB.

To obtain YSZ, zirconia (ZrO_2) is doped with yttria (Y_2O_3), thereby creating oxygen vacancies [16], which play a role in the ionic conductivity, where it is well known that the conductivity is maximised at a Y_2O_3 concentration of around 8% [17]. In addition, experimental [18–20] and theoretical [21,22] studies have shown that the dopant (Y^{3+}) is located preferentially at the next nearest neighbour (NNN) site to the oxygen vacancy. We will therefore concentrate on the configuration with the dopant in the NNN site in our model of the YSZ cermet.

Several ab initio investigations have been carried out on the interaction of molecules with the Ni/YSZ cermet [23–26]. Shishkin et al. [23] showed the oxidation of hydrogen at the TPB by the oxygen atoms bound to Zr (or Y) and Ni. Cucinotta et al. [24] showed that the hydrogen oxidation can be active away from the TPB, when water is adsorbed on the oxide surface. Ammal et al. [25] combined DFT and microkinetic studies to show that the O migration pathway is faster than the H spillover and OH migration pathway. Shishkin and Ziegler [26] have studied the oxidation of H_2, CH_4 and CO at the Ni/YSZ interface and showed that the YSZ cermet is inert to fuel oxidation, while Ni is active towards fuel adsorption and oxidation. However, a systematic characterization of H_2O, CO_2 and CO molecules at the TPB is still missing. We have therefore investigated the interaction of these three molecules on four relevant surfaces, i.e. ZrO_2(111), Ni/ZrO_2(111), YSZ(111) and Ni/YSZ(111), and compared our results with experimental data.

We have investigated up to five initial adsorption sites for each molecule on the pristine surfaces (ZrO_2(111) and YSZ(111)) and two more on the surfaces with supported Ni (Ni/ZrO_2(111) and Ni/YSZ(111)). We have elucidated the geometries and electronic structures of the most stable adsorption sites and compared these results with other reported computational models, where available, and supported our findings by experimental and computational infrared spectra (IR).

2. Models and computational methods

All the structural relaxations and frequency calculations have been performed using the Vienna Ab-initio Simulation Package (VASP) [27–30], solving the Kohn-Sham equations of the density functional theory (DFT) [31] in a periodic approximation. The calculations have been carried out adopting the generalized gradient approximation (GGA) [32] with the Perdew-Burke-Ernzerhof (PBE) density functional. The semi-empirical method of Grimme [33] was employed to describe and improve the long-range dispersion interactions. The H (1 s), C (2 s, 2 p), O (2 s, 2 p), Ni (3 d, 4 s), Zr (4 d, 5 s) and Y (4 s 4p 4 d 5 s) atomic orbitals have been treated as valence electrons, while the remaining electrons were considered as core electrons and kept frozen. To describe the interaction between the valence and the core electrons, we adopted the projected augmented wave method (PAW) [34]. The plane-waves kinetic energy cutoff was fixed at 500 eV, and all the calculations were spin-polarized. The conjugate gradient technique has been used for the geometry optimizations with an interatomic force threshold of 0.01 eV/Å. Monkhorst-Pack grids with a $7 \times 7 \times 1$ k-point mesh were used to sample the reciprocal space for the 1×1 slab calculations. For the molecules in the gas phase a $1 \times 1 \times 1$ mesh of k-points was used and each molecule was positioned in a large box ($14 \times 15 \times 16$ Å^3) in order to avoid lateral interactions. The rest of the settings were similar to those used for the slab calculations.

The procedure to compute the vibrational frequencies is implemented in the VASP software. The vibrational frequencies were evaluated by finite displacements of every coordinate and the vibrational frequencies thus correspond to the eigenvalues of the diagonal Hessian matrix (second derivative of the energy with respect to the atomic positions), where the eigenvectors are the vibrational normal modes of the system. Frequency changes reflect a structural modification of the molecules upon adsorption on the surfaces.

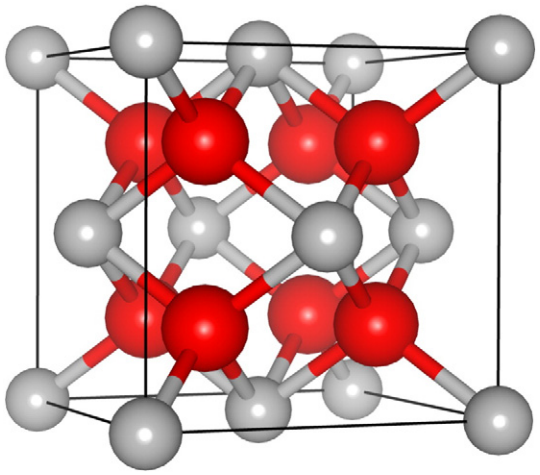

Fig. 1. Crystal structure of cubic zirconia (c-ZrO_2). Colour key: oxygen and zirconium atoms are represented by red and grey spheres, respectively. (For interpretation of the references to colour in this figure legend, the reader is referred to the web version of this article.)

In Fig. 1 we show the fluorite crystal structure of cubic zirconia (c-ZrO_2), the unit cell of which is face cantered cubic (fcc) (space group *Fm*-3m). The fcc cube is formed by the Zr atoms which are coordinated to eight oxygens. The oxygen atoms are positioned on the diagonals of the cube.

To describe the (111) surfaces we have used a slab model with a perpendicular vacuum size of 15 Å, i.e. large enough to avoid interactions with its periodic images. Following previous work [22,35], the surfaces were O-terminated and contained 9 atomic layers (three O-Zr-O trilayers); the 5 top atomic layers were allowed to relax fully during geometry optimization, while the 4 layers at the bottom were kept fixed, thereby simulating the bulk material. The surface area is 44.96 Å^2.

The four surfaces (ZrO_2(111), Ni/ZrO_2(111), YSZ(111) and Ni/YSZ(111)) were taken from our previous work [22]. There, we had substituted two Zr (from the topmost and the sub-surface O-Zr-O trilayers) by Y with the removal of one oxygen from the third atomic layer (the next nearest neighbour of Y atoms) to obtain the YSZ(111) surface ($Zr_{10}Y_2O_{23}$(111) slab) (yttria = 9.1 wt%). Then, Ni was deposited on the most favourable adsorption site on both the ZrO_2(111) and YSZ(111) surfaces. On the ZrO_2(111) surface, Ni sits preferentially on the O_d' atom, i.e. slightly off from the perpendicular, Fig. 2, while on the YSZ(111), it adsorbs preferentially on top of the oxygen vacancy and away from the Y atoms (Fig. 2).

The magnetization of the Ni atom before adsorption was 0.57 μ_B (Ni atom from bulk calculation). Upon adsorption on both ZrO_2(111) and YSZ(111) surfaces, the calculated magnetisation for the adsorbed Ni atom was 0.0 μ_B (singlet configuration). For comparison, we have also forced the Ni atom to be in a triplet configuration (2.0 μ_B) and the calculated total energies were 1.16 and 1.44 eV higher for Ni/ZrO_2(111) and Ni/YSZ(111), respectively, compared with the values found for the singlet configuration. Moreover, a study made by Hahn et al. [36] took into account different spin states of Ni_{10} cluster adsorbed on CeO_2(111) surface and they showed that the singlet configuration of the cluster is stable, as it is only 0.01 eV higher in energy than the configuration where the multiplicity is 11.

The three molecules (H_2O, CO and CO_2) were initially positioned at 2.0 Å above the surface and different orientations have been compared for each initial adsorption site. On the ZrO_2(111) surfaces, four initial adsorption sites were tested for each molecule: on top of the Zr atom, above the outermost oxygen O_u (up) or O_d (down), and finally at the centre of the O_u-O_d-Zr "triangle", see Fig. 2. On the YSZ(111) surface,

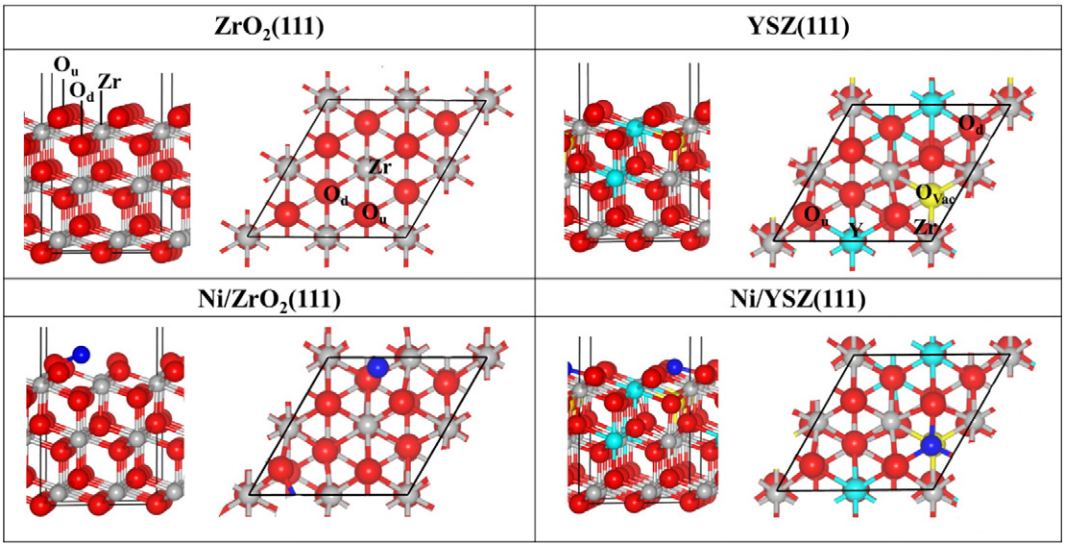

Fig. 2. Side and top views of the O-terminated ZrO_2(111), YSZ(111), Ni/ZrO_2(111) and Ni/YSZ(111) surfaces. Red, grey, blue and cyan spheres represent oxygen, zirconium, nickel, and yttrium atoms, respectively. The oxygen vacancy is represented by the yellow sphere. (For interpretation of the references to colour in this figure legend, the reader is referred to the web version of this article.)

six initial adsorption sites were investigated: the Zr atom, the outermost oxygen O_u (up), O_d (down), the oxygen vacancy, the yttrium atom, and the centre of the O_u-O_d-Zr "triangle", see Fig. 2. For each initial adsorption site, we have relaxed the molecules, as well as the five top layers of the slab (as described in the previous paragraph). On the Ni/ZrO_2(111) and Ni/YSZ(111) surfaces, we identified two initial adsorption sites: near the Ni atom and approximately over the most stable adsorption site found for the naked surface. The non-equivalent initial adsorption sites leading to unstable configurations are presented in the supporting information. We have calculated the adsorption energy, taking into account the zero point energy (ZPE), as the difference between the energy of the slab with the molecule adsorbed ($E_{molecule/surface}$) and the sum of the energies of the clean oxide surface ($E_{surface}$) and the isolated molecule ($E_{molecule}$), Eq. (1).

$$E_{ads} = E_{molecule/surface} - (E_{surface} + E_{molecule}) \quad (1)$$

We have also calculated the Van der Waals adsorption energies as the difference between the estimated Van der Waals energy of the slab with the molecule adsorbed ($E^{vdW}_{molecule/surface}$) and the sum of the estimated Van der Waals energies of the clean oxide surface ($E^{vdW}_{surface}$) and the isolated molecule ($E^{vdW}_{molecule}$), Eq. (2).

$$E^{vdW}_{ads} = E^{vdW}_{molecule/surface} - \left(E^{vdW}_{surface} + E^{vdW}_{molecule}\right) \quad (2)$$

We have analysed the charge transfer between the surface and the molecules using Bader analysis as implemented in the Henkelman algorithm [37]. To evaluate the interaction between the molecules and the surface atoms we have also calculated the electron localization function (ELF) which measures the probability of finding an electron in the neighbourhood of another electron with the same spin [38].

3. Results and discussion

3.1. Structural analysis and electronic structure

3.1.1. ZrO_2(111)

The evaluation of the adsorption energies for the three molecules shows that the strength of their adsorption on the ZrO_2(111) surface follows the trend: $H_2O > CO > CO_2$ (see Table 1). H_2O is likely to be dissociated, where one H is transferred to a surface oxygen with the OH remaining on top of the Zr atom (Fig. 3). The dissociative water adsorption on ZrO_2 was also observed in a previous investigation by Korhonen et al. [39], where they showed experimentally and theoretically that water, at low coverage, dissociates on the monoclinic zirconia surface. Our calculated adsorption energy on c-ZrO_2 for [H + OH]-ZrO_2(111) (−1.08 eV) is similar to the adsorption on their monoclinic $(\bar{1}11)$ and the $(\bar{1}01)$ zirconia surfaces (−1.20 eV).

The most stable adsorption site found for CO_2 and CO molecules is on top of the zirconium atom (Fig. 3). The adsorption energy for CO_2 on ZrO_2(111) (−0.24 eV) is close to a previous study (−0.26 eV) [40], where the authors had modelled the zirconia surface by four types of clusters and saturated the dangling bonds with hydrogen atoms: $Zr_2O_{14}H_{20}$, $Zr_3O_{16}H_{20}$, $Zr_3O_{19}H_{26}$ and $Zr_5O_{24}H_{28}$ (see Fig. S5 in SI). The $Zr_2O_{14}H_{20}$ and $Zr_3O_{19}H_{26}$ exhibit OH groups, while in $Zr_3O_{16}H_{20}$ and $Zr_5O_{24}H_{28}$ only H atoms are adsorbed on the oxygen clusters. The main difference between $Zr_3O_{16}H_{20}$ and $Zr_5O_{24}H_{28}$ is the Zr atom pointing outwards from the $Zr_5O_{24}H_{28}$ cluster. For $Zr_3O_{16}H_{20}$ the calculated CO_2 adsorption energy was −0.26 eV (similar to this work) and the authors [40] showed that CO_2 is physisorbed at 2.70 Å away from the cluster and adopting a parallel position, comparable to our geometry (Fig. 3). On top of the $Zr_2O_{14}H_{20}$ and $Zr_3O_{19}H_{26}$ clusters, the authors [40] found a stronger CO_2 adsorption energy (−0.34 and −0.35 eV, respectively), but CO_2 is still physisorbed since for both clusters the CO_2-cluster distance remains larger than 2.10 Å, indicating that the OH groups play a minor role in the CO_2 adsorption. On top of $Zr_5O_{24}H_{28}$ the CO_2 adsorption was much stronger (−0.67 eV) but the authors showed, using the multi-Langmuir model, that the $Zr_5O_{24}H_{28}$ site is less abundant than the three other sites. Thus, at high CO_2 loading, the authors [40] concluded that CO_2 adsorbs onto the $Zr_2O_{14}H_{20}$,

Table 1
Calculated adsorption energies per molecule (E_{ads} in eV) and charges (q in e^-) for the molecules (H_2O, CO_2 and CO) adsorbed on the most favourable site of the surfaces: ZrO_2(111), Ni/ZrO_2(111), YSZ(111) and Ni/YSZ(111).

	ZrO_2(111)	Ni/ZrO_2(111)	YSZ(111)	Ni/YSZ(111)
$E_{ads}(H_2O)$	--	-1.39	-0.82	-0.67
E_{ads}(H+OH)	-1.08	-1.33	-0.30	-0.52
$E_{ads}(CO_2)$	-0.24	-1.35	-0.36	-0.31
E_{ads}(CO)	-0.37	-2.70	-0.37	-2.32
	ZrO_2(111)	Ni/ZrO_2(111)	YSZ(111)	Ni/YSZ(111)
q(H+OH)	0.1	--	--	--
q(H_2O)	--	0.0	0.0	0.0
q(CO_2)	0.0	-0.5	0.0	0.0
q(CO)	0.0	-0.2	0.0	-0.3

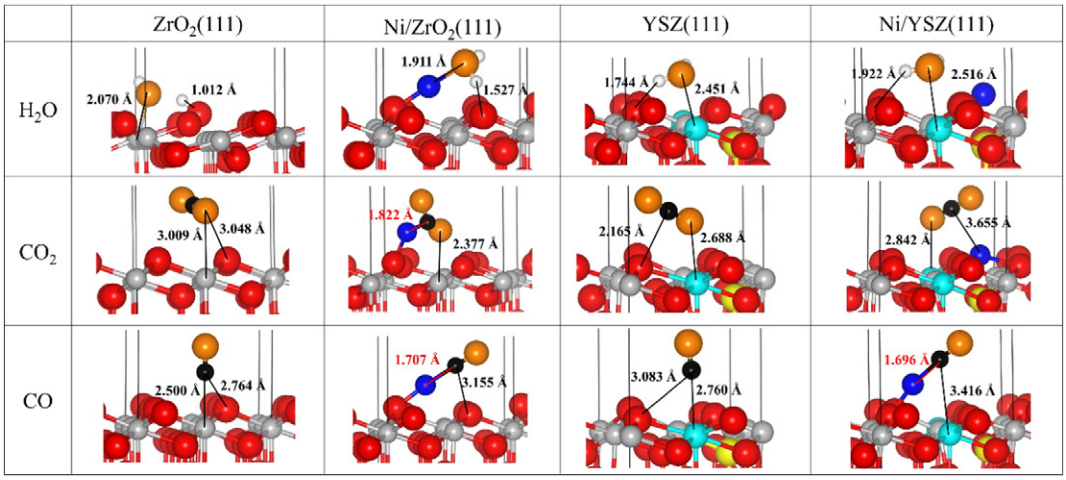

Fig. 3. Schematic representation of the H_2O, CO_2 and CO adsorption on $ZrO_2(111)$, $Ni/ZrO_2(111)$, YSZ(111) and Ni/YSZ(111). Perpendicular black lines show the simulation cell. Red, grey, blue and cyan spheres represent oxygen, zirconium, nickel, and yttrium atoms, respectively. Orange spheres represent the oxygen belonging to CO and CO_2 molecules. The oxygen vacancy is represented by the yellow spheres. (For interpretation of the references to colour in this figure legend, the reader is referred to the web version of this article.)

$Zr_3O_{16}H_{20}$ and $Zr_3O_{19}H_{26}$ clusters. In our study, the most stable adsorption found for CO on $ZrO_2(111)$ is stronger (−0.37 eV) than the one on O_d suggested by Walter et al. [41] (−0.14 eV), which in our model was evaluated to be −0.10 eV.

Among the three molecules, dissociated H_2O has a stronger affinity for the $ZrO_2(111)$ surface than CO_2 and CO. The variation of the interatomic distances is in good agreement with the adsorption energies and the transferred charges (see Table 1). For instance, [H + OH] is the closest species to the $ZrO_2(111)$ surface. Fig. 3 shows that O (of OH) is at 2.070 Å over the top zirconium atomic layer, while the closest atom, O for CO_2 and C for CO, are positioned at 3.009 Å and 2.500 Å, respectively, from the surface which, added to a lack of charge transfer, suggests that both molecules are physisorbed.

3.1.2. Ni/ZrO2(111)

On the $Ni/ZrO_2(111)$ surface, the strength of adsorption of the molecules near Ni is as follow: CO > H_2O > CO_2. Table 1 shows that, depending on the activation energies, H_2O dissociation is practically in equilibrium with molecular adsorption since $E_{ads}(H_2O)$-Ni/$ZrO_2(111)$ ~ E_{ads}[H + OH]-Ni/$ZrO_2(111)$ (−1.39 and −1.33 eV respectively). The adsorption energy of CO_2 (−1.35 eV) is similar to H_2O but considerably weaker than the one found for CO (−2.70 eV), which will surround the single atom, replacing both CO_2 and H_2O.

There is no obvious change in the H_2O intra-molecular bond distances. However, the intra-molecular CO_2 bond length increases from 1.2 Å (gas phase) to 1.3 Å (CO_2-Ni/$ZrO_2(111)$) and the CO bond length increases from 1.1 Å to 1.2 Å (CO-Ni/$ZrO_2(111)$). A previous study also reported these elongations of the intra-molecular distances upon interaction of the molecules with supported metal cluster on oxide surfaces [42]. Meanwhile, H_2O remains practically unaltered, whereas CO_2 and CO indicate an electronic rearrangement which is not seen on the bare $ZrO_2(111)$. Charge analysis shows a gain of charge for CO_2 ($-0.5\ e^-$) and CO ($-0.2\ e^-$) upon adsorption on the $Ni/ZrO_2(111)$. The outermost Zr atomic layer and the Ni atom lose $+0.3\ e^-$ and $+0.2\ e^-$, respectively, while for CO-Ni/$ZrO_2(111)$ only the outermost Zr atomic layer transfers $+0.2\ e^-$, through the Ni adatom, to the CO molecule.

The electron localization function (ELF) plots in Fig. 4 show the effect of the Ni on the molecules' adsorption onto the surface. In the H_2O-Ni/$ZrO_2(111)$ case, the electron localization is negligible between H and the oxygen belonging to the surface, whereas the electrons localized on the oxygen atom of the water molecule interact favourably with the empty orbitals of the Ni atom, showing that Ni facilitates the adsorption of H_2O on the $Ni/ZrO_2(111)$ surface. In Fig. 4 we note a bonding region between CO_2 and Ni, which is not observed in the CO_2-$ZrO_2(111)$ system. This interaction explains the strengthening of the CO_2 adsorption over $Ni/ZrO_2(111)$ compared to the bare $ZrO_2(111)$ surface. The shape of the ELF around the carbon atom from CO changes in the presence of Ni: it points towards the Ni atom, showing the important effect of the metal atom.

In Fig. 5 we show the total density of states (DOS) of the three molecules (H_2O, CO_2 and CO) adsorbed on $ZrO_2(111)$ and $Ni/ZrO_2(111)$ and the projected DOS on the three relevant atoms (C, O and H) and the Ni atom. A sharp peak (specific orbital) means that a specific orbital is located at this specific energy. Thus, when many orbitals of different atoms have the same energy (well localized) we consider that the interaction between those orbital atoms is favourable. On the other hand, the interaction is unfavourable if the peaks of the different orbital atoms are spread over a range of energies (delocalized).

We have shown, in the [H + OH]/$ZrO_2(111)$ density of states (DOS) (Fig. 5), that the peaks located below the Fermi energy correspond to the s and p orbitals of OH oxygen and are delocalized. However, in the H_2O-Ni/$ZrO_2(111)$ system, they are localized and positioned at the same energy as the final two Ni s p d orbital peaks (−0.26, −0.20 and −0.01 eV). This favours the interaction between the Ni atom and the H_2O oxygen orbitals which is in good agreement with the ELF analysis.

Similar situations occur with the CO_2 and CO molecules, i.e. their orbitals below the Fermi energy are dispersed over a range of energies when interacting with a naked surface, but are localized peaks in the presence of Ni atoms. The peaks at these energies correspond to Ni, O and C orbitals, indicating that an interaction exists between the molecule and $Ni/ZrO_2(111)$ and that this interaction is facilitated by the Ni atom, which confirms the ELF analysis discussed above.

We have shown that the adsorption of the molecules on $ZrO_2(111)$ and $Ni/ZrO_2(111)$ can lead to the dissociation of H_2O, and causes the elongation of the intramolecular bonds of CO and CO_2. In addition, the ELF plot indicates the significant effect of Ni on the electronic structure of the molecules, thereby enhancing their chemisorption. These results are in agreement with previous investigations, which have shown that metal particles can stabilize the adsorption of the molecule on the surface [43–46]. For example, Carrasco et al. [47] showed that CO prefers to bind to the $Ni_1/CeO_2(111)$ surface, rather than on the pristine $CeO_2(111)$ surface, in a similar configuration as the one presented in Fig. 3.

3.1.3. YSZ(111)

We have followed the same procedure on the ~9% yttria-doped $ZrO_2(111)$. The adsorption energies of these molecules on the YSZ(111) shows the following preference for binding: H_2O > CO > CO_2, see

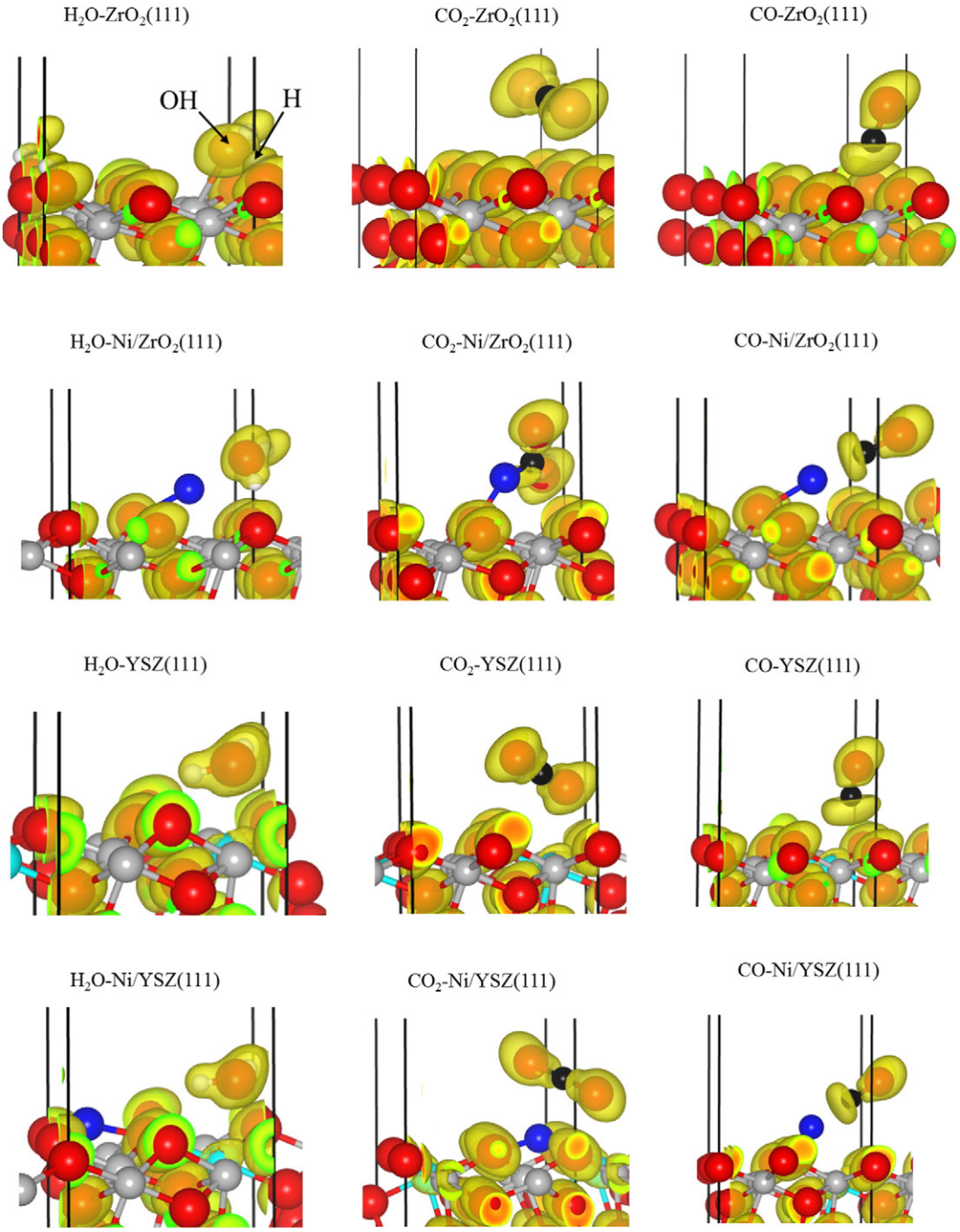

Fig. 4. Electron localization function (ELF) of the three molecules (H_2O, CO_2 and CO) adsorbed on top of the four surfaces: $ZrO_2(111)$, $Ni/ZrO_2(111)$, YSZ(111) and Ni/YSZ(111). A high ELF value along the bond path reflects a strong interaction between the molecule and the surface while a low ELF value is the consequence of a weak interaction.

Table 1. Unlike the water adsorption on $ZrO_2(111)$, H_2O prefers to remain as a molecule on YSZ(111) since $E_{ads}(H_2O)$-YSZ(111) is more favourable than $E_{ads}(H + OH)$-YSZ(111) by ~0.5 eV, see Table 1. The CO_2 adsorption becomes ~0.1 eV stronger compared with the pristine $ZrO_2(111)$. Both H_2O and CO_2 adsorb near the yttrium atom in a slightly tilted position, whereas CO binds perpendicularly to the surface (Fig. 3). The CO adsorption energy is −0.37 eV, i.e. very close to the one on $ZrO_2(111)$ and in good agreement with the DFT study by Yurkiv et al. (−0.34 eV) [48].

The analysis of the interatomic distances from the structures in Fig. 3 agrees with the trend in adsorption energies, since H_2O is stabilized by H bonds with the surface ($H\text{-}O_{surf}$ = 1.744 Å), and CO_2 and CO are not strongly bound. There is negligible variation in the intra-molecular distances or charge transfer for any of the three molecules. The electronic structure and the charge transfer compared with the pristine $ZrO_2(111)$ indicate that the interaction of CO_2 and CO molecules is barely modified by the presence of Y-dopants. However, H_2O prefers to adsorb molecularly on the YSZ(111) surface, whereas it dissociates upon adsorption on the $ZrO_2(111)$ surface.

3.1.4. Ni/YSZ(111)

Once Ni is deposited on YSZ(111), the trend in the adsorption of the molecules changes from the naked surface and the preference becomes: CO > H_2O > CO_2. As on YSZ(111), H_2O adsorbs molecularly on Ni/YSZ(111), although the difference in adsorption energy compared to the

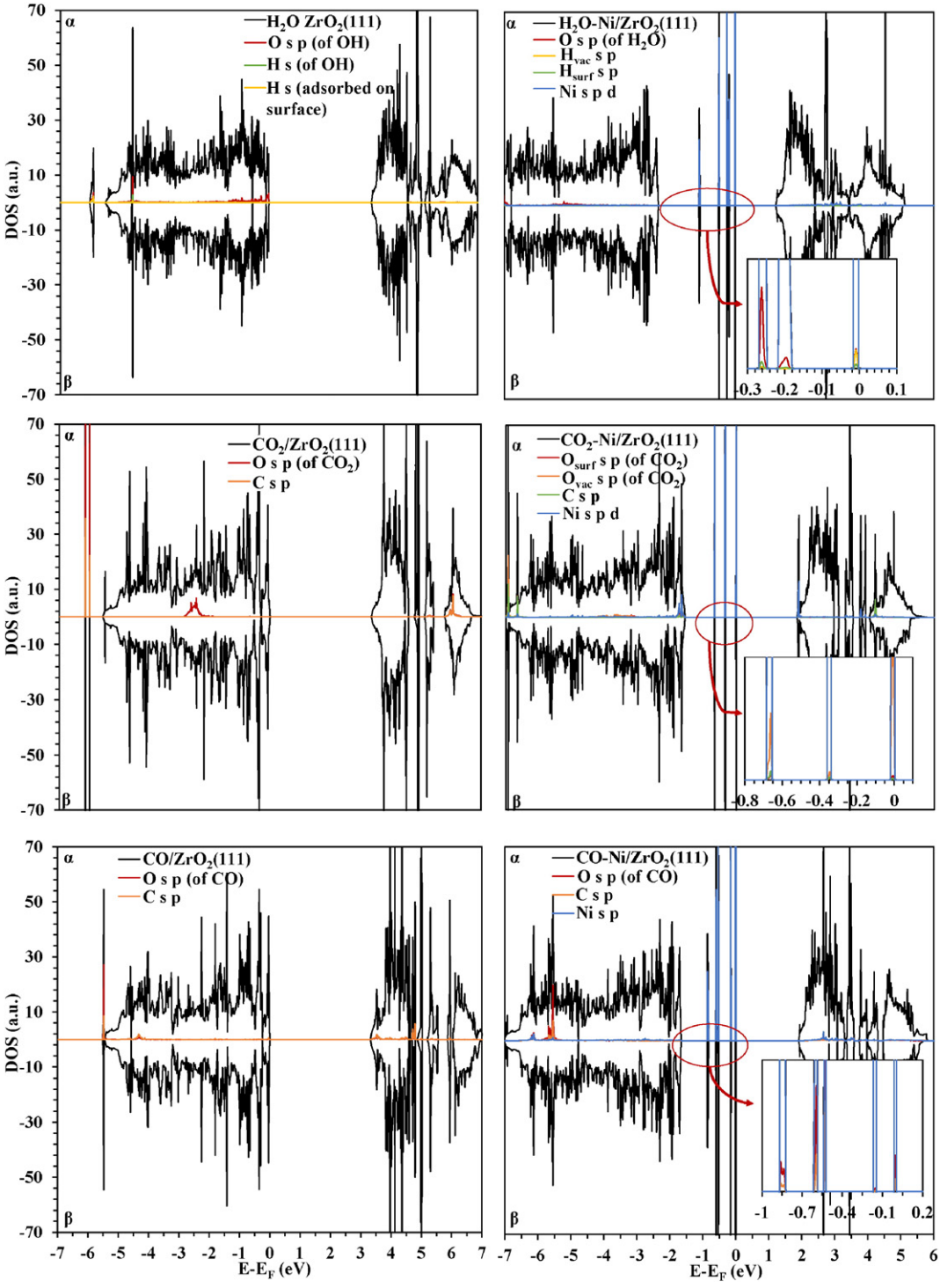

Fig. 5. Total density of states (DOS) of the three molecules (H_2O, CO_2 and CO) adsorbed on ZrO_2(111) and Ni/ZrO_2(111) and projected DOS on the three molecule atoms (C, O and H) and Ni atom. We represent here both spin up (α) and down (β) of the total DOS and the spin up for the projected DOS. Colour scheme is labelled in the inset. H_{vac} and H_{surf} correspond to H pointing towards the vacuum and the surface, respectively. The oxygen pointing towards the vacuum and the surface are represented by O_{vac} and O_{surf}, respectively.

dissociated configuration is only 0.15 eV, indicating a close thermodynamic equilibrium (depending on the energy barrier to dissociation). H_2O adsorbs near the Y and away from Ni, while CO_2 and CO prefer to adsorb near the Ni atom with adsorption energies of −0.31 and −2.32 eV respectively. Only CO has more affinity for the Ni/YSZ(111) surface than for YSZ(111), releasing almost 2 eV more than on the bare YSZ(111) surface. Thus, as a general trend, H_2O and CO_2 adsorb on the bare surface, while CO is strongly attached to Ni/YSZ(111), see Table 1.

The distance analysis of the structures in Fig. 3 shows that H_2O and CO_2 are at approximately 2.0 Å from the surface, while the C atom (of CO) is 1.696 Å from the Ni atom. There is no obvious increase in either H_2O or CO_2 intra-molecular bond lengths. However, the CO bond increases by 0.1 Å upon adsorption, in agreement with the strong adsorption and the charge transfer of −0.3 e^- from the outermost zirconium atomic layer. As such, Ni acts as an electrode, which is its main function in SOFC: electrons are transferred from

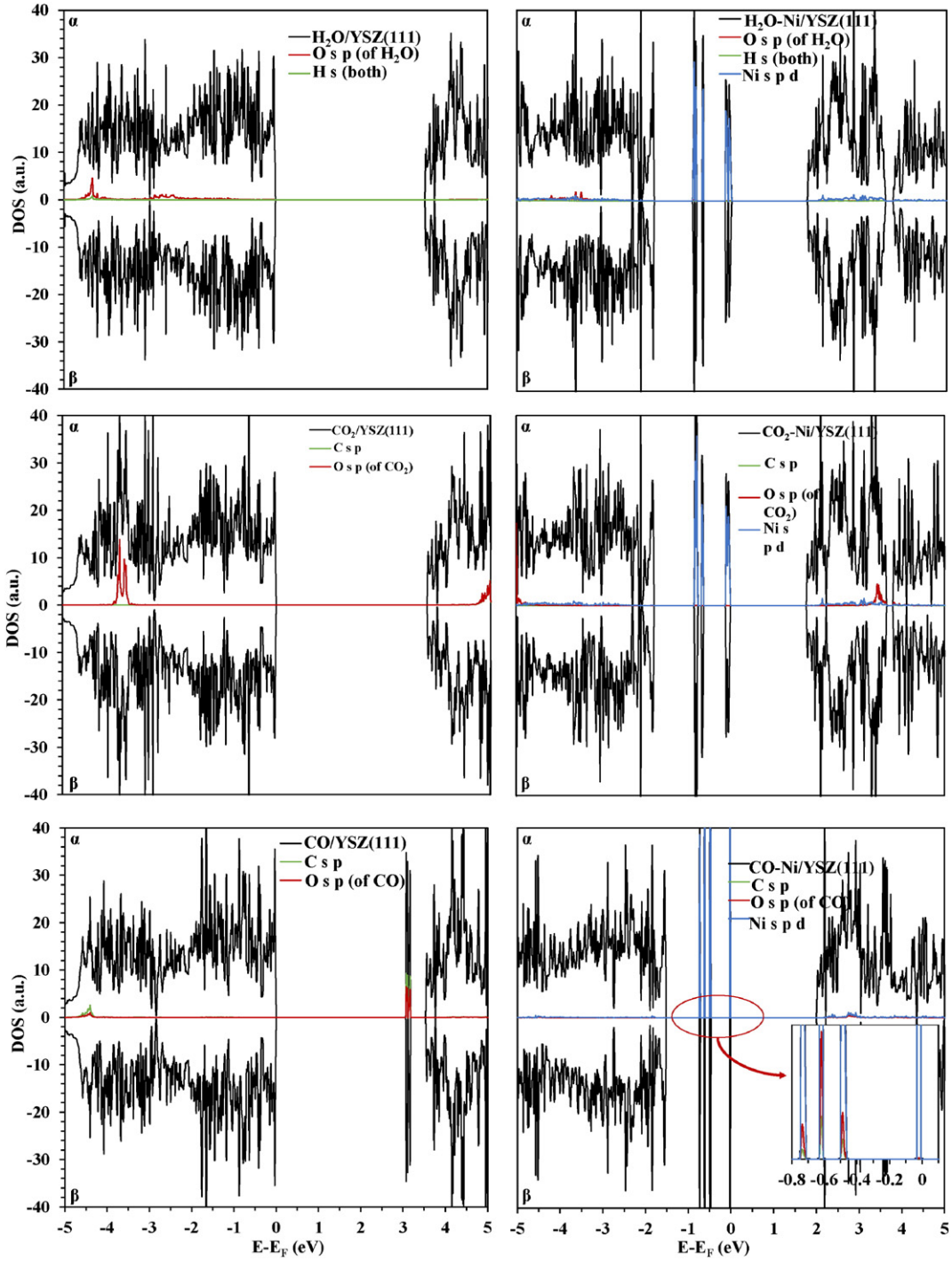

Fig. 6. Total density of states (DOS) of the three molecules (H_2O, CO_2 and CO) adsorbed on YSZ(111) and Ni/YSZ(111) surfaces and projected DOS on the three molecule atoms (C, O and H) and Ni atom. We represent here both spin up (α) and down (β) of the total DOS and the spin up for the projected DOS. Colour scheme is labelled in the inset. (For interpretation of the references to color in this figure legend, the reader is referred to the web version of this article.)

the surface through Ni. The other molecules remain neutral upon adsorption.

To investigate further the role of Ni, we have compared the ELF for the YSZ(111) and Ni/YSZ(111) systems. Fig. 4 shows that the perturbation of the ELF upon adsorption of H_2O and CO_2 is negligible, which agrees with physisorption and the insignificant effect of Ni. However, the perturbation of the electrons surrounding the CO molecule is considerable in the presence of Ni.

In the H_2O-Ni/YSZ(111) DOS (Fig. 6) we observe five localized peaks (−0.89, −0.85, −0.67, −0.12 and −0.04 eV) below the Fermi level, corresponding to the Ni s p d orbitals. The contribution of the H_2O orbitals to these peaks is negligible, indicating that H_2O interacts weakly with both YSZ(111) and Ni/YSZ(111) surfaces, in good agreement with the low adsorption energies and the ELF analysis. The conclusion is similar for the CO_2/YSZ(111) and CO_2-Ni/YSZ(111) systems, where the DOS plots show that the CO_2 orbitals do not contribute to the valence band, in agreement with the weak adsorption and the ELF plots. However, the presence of Ni causes the CO orbitals to be localized at the same energy as the Ni orbitals below the Fermi level (−0.72, −0.62, and −0.48 eV), leading to a stronger interaction. Thus, Ni stabilizes CO adsorption on the Ni/YSZ(111) surface, as was also observed from the ELF analysis.

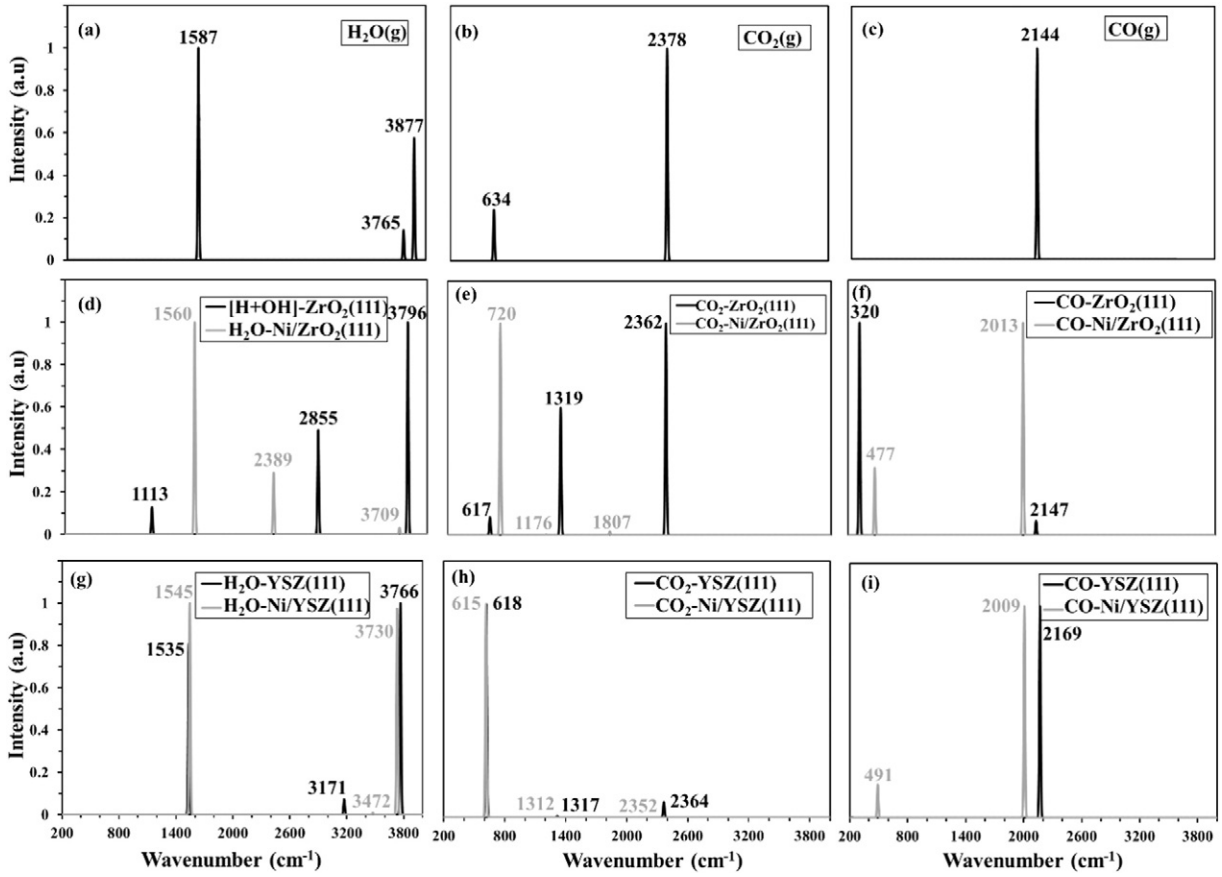

Fig. 7. Theoretical IR spectra of the free and adsorbed molecules (H_2O, CO_2 and CO) on ZrO_2(111), Ni/ZrO_2(111), YSZ(111) and Ni/YSZ(111). (For interpretation of the references to colour in this figure legend, the reader is referred to the web version of this article.)

3.2. Infrared spectra

We have calculated and analysed the IR spectra of the three molecules in the gas phase and compared them with the molecules adsorbed on the four surfaces (Fig. 7), which provides data that are directly comparable with simple experimental characterization, thus providing circumstantial evidence of the geometries and electronic structures described above.

Table 2
Theoretical vibrational frequencies (ω) in cm^{-1} for H_2O, CO_2 and CO in the gas phase and adsorbed on the surfaces (ZrO_2(111), Ni/ZrO_2(111), YSZ(111) and Ni/YSZ(111). ν, ν_s, ν_{as}, and δ denote stretching, symmetrical stretching, asymmetrical stretching and bending modes, respectively. We show in parenthesis the infra-red experimental values from the literature.

	H_2O		CO_2		CO	
	assignment	ω	assignment	ω	assignment	ω
Gas Phase	ν_s	3765 (3657[51])	ν_s	1324	ν	2144 (2142[52])
	ν_{as}	3877 (3756[51])	ν_{as}	2378 (2349[51])		
	δ	1587 (1595[51])	δ	634 (667[51])		
ZrO_2(111)	ν(H-$O_{surface}$)	2855	ν_s	1319	ν	2147 (2185[53])
	ν(H-O_{water})	3796	ν_{as}	2362	δ	320
	δ of both H	1113	δ	617		
Ni/ZrO_2(111)	ν of H-O_{water}(H toward surface)	2389	ν_s	1176	ν	2013
	ν of H-O_{water}(H toward vacuum)	3709	ν_{as}	1807	δ	477
	δ of both H	1560	δ	720		
YSZ(111)	ν_s	3171	ν_s	1317	ν	2169
	ν_{as}	3766	ν_{as}	2364	δ	224
	δ	1535	δ	618		
Ni/YSZ(111)	ν_s	3472	ν_s	1312	ν	2009
	ν_{as}	3730	ν_{as}	2352	δ	491
	δ	1545	δ	615		

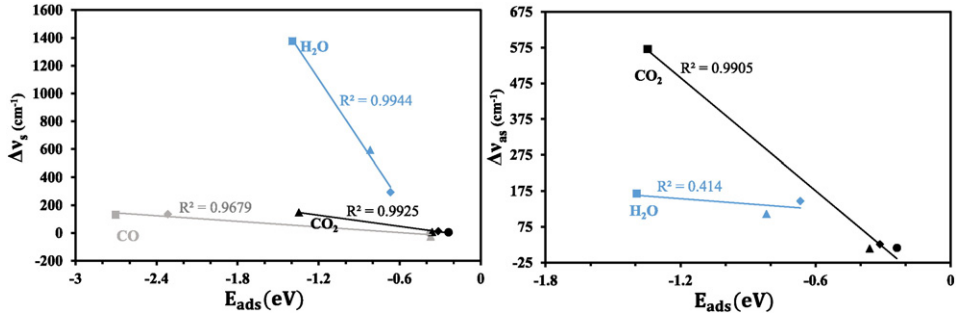

Fig. 8. Plot of the variation of the symmetric (ν_s) and asymmetric (ν_{as}) stretching modes upon adsorption. ●, ■, ▲ and ♦ represent $ZrO_2(111)$, $Ni/ZrO_2(111)$, YSZ(111) and Ni/YSZ(111) surfaces, respectively. E_{ads} corresponds to the total adsorption energy. Since H_2O adsorbs dissociatively on $ZrO_2(111)$ the variation of H_2O stretching mode on $ZrO_2(111)$ is not represented here. ν_{as} is not represented for CO as in the gas phase CO has one stretching mode.

For example, the molecularly adsorbed water is confirmed by the presence of a bending mode around 1600 cm^{-1}, since there is no OH-related vibrational mode at 1600 cm^{-1} [49]. Similarly, analysing the IR spectra of adsorbed CO_2 and CO indicates a potential dissociative chemisorption of CO_2, as was shown by previous studies where CO_2 is adsorbed on top of silica-supported iron [50]. In Table 2 we show the IR spectra values related to Fig. 7 and compare them with the experimental values from the literature [51,52].

3.2.1. $ZrO_2(111)$ and $Ni/ZrO_2(111)$

The wavenumbers of the vibrational modes of the water molecule drop upon adsorption on both the $ZrO_2(111)$ and $Ni/ZrO_2(111)$ surfaces. A drop of the bending mode is observed ($\Delta\delta_{H_2O-ZrO_2(111)} = 474\ cm^{-1}$) upon H_2O adsorption on the $ZrO_2(111)$ surface compared to the gas phase, but since H_2O adsorption is dissociative on $ZrO_2(111)$ the bending mode observed in [H + OH]-$ZrO_2(111)$ actually corresponds to the bending mode of both hydrogens: the H transferred to the surface and the H bonded to O_{water}. This frequency variation of the bending mode was expected, since upon adsorption the H—O_{water} and H—O_{surf} bonds are weaker than the H—O bonds in the water molecule in vacuum. Similarly to [H + OH]-$ZrO_2(111)$, there are two different stretching modes, one each corresponding to ν(H—O_{surf}) and ν(H—O_{water}). In addition, Table 2 shows, that from these stretching modes ν(H—O_{surf}) has the lowest wavenumber, which is predictable since the H—O_{surf} bond is weaker than H—O_{water}. The wavenumber of the two stretching modes of H_2O over $Ni/ZrO_2(111)$ are even lower than the ones found for $ZrO_2(111)$. This is in good agreement with the larger adsorption energy of H_2O-$Ni/ZrO_2(111)$: H_2O binds more strongly to $Ni/ZrO_2(111)$ than $ZrO_2(111)$, which weakens its internal bonding by electronic rearrangement, explaining the decrease of the stretching modes of H_2O-$Ni/ZrO_2(111)$.

The adsorption of CO_2 is weak on $ZrO_2(111)$, with the wavenumbers of the three different vibrational modes remaining similar to the gas phase (Table 2). However, it adsorbs strongly on $Ni/ZrO_2(111)$, lowering the wavenumbers of the asymmetrical and symmetrical stretching modes by 571 and 148 cm^{-1}, respectively. Indeed, the stronger adsorption of CO_2 on top of $Ni/ZrO_2(111)$ affects the strength of the CO_2 bonds, which explains the drop of the wavenumbers of the stretching modes observed in CO_2-$Ni/ZrO_2(111)$. The bending mode of CO_2-$Ni/ZrO_2(111)$ increases by 103 cm^{-1} compared to CO_2-$ZrO_2(111)$. The reason for this increase is explained by the rearrangement of the electronic structure of CO_2 upon adsorption on $Ni/ZrO_2(111)$, where CO_2 gains a charge of 0.5 e^-. As to CO, the difference in stretching mode upon adsorption on $ZrO_2(111)$ is negligible compared with the gas phase: $\Delta\nu_{CO-ZrO_2(111)} = -3\ cm^{-1}$, confirming the physisorbed state, which is in good agreement with the experimental study made by Dulaurent et al. [53] (ν(CO) = 2185 cm^{-1}). On $Ni/ZrO_2(111)$, the wavenumber of the stretching mode is even lower ($\Delta\nu_{CO-Ni/ZrO_2(111)} = 131\ cm^{-1}$), in good agreement with the strong adsorption energy and increase of the C—O distance.

3.2.2. YSZ(111) and Ni/YSZ(111)

Vibrational modes of H_2O on YSZ(111) and Ni/YSZ(111) show a decrease in wavenumbers compared to the gas phase, although they remain higher than on $ZrO_2(111)$. The asymmetrical and symmetrical stretching and bending modes of H_2O are located at lower wavenumber, when it is adsorbed on YSZ(111) and on Ni/YSZ(111) (Table 2). This analysis agrees with the weakness of the intramolecular bonds on both doped surfaces, as described before.

CO_2 adsorbs on both YSZ(111) and Ni/YSZ(111) surfaces, leading to a decrease in the wavenumber of each vibrational mode (Table 2). These shifts of the vibrational modes upon adsorption are related to the decreased strength of CO_2 bonds due to the interaction with the surfaces and the occupation of the molecular antibonding orbitals leading to a bent structure. Our calculated value for the symmetrical stretching mode of CO_2 on YSZ(111) (1317 cm^{-1}) is in the same range as the experimental study made by Köck et al. [54], who found a peak of a bridged carbonate at 1305 cm^{-1}. The adsorption energies of CO-YSZ(111) and CO-Ni/YSZ(111) agree with the CO affinity for these two surfaces. For example, on Ni/YSZ(111) the stretching mode of the CO molecule is observed at significant lower wavenumber than in the gas phase (Table 2), having decreased by 135 cm^{-1}. The increase in the length of the CO bond upon adsorption and its weakening further shows the strong interaction between CO and the bare and Ni-decorated YSZ surfaces.

To summarize the general trend of the vibrational modes of the molecules upon adsorption, we have plotted in Fig. 8 the variation of the stretching modes as a function of the adsorption energies. Note that the H_2O dissociation is not represented here. We have observed that,

Table 3
Calculated E_{ads} and ($E_{ads} - E_{ads}^{vdW}$) in eV for the three molecules (H_2O, CO_2 and CO) adsorbed on the most favourable site of the surfaces: $ZrO_2(111)$, $Ni/ZrO_2(111)$, YSZ(111) and Ni/YSZ(111). E_{ads} and E_{ads}^{vdW} correspond to the total and Van der Waals adsorption energies, respectively.

	H_2O		CO_2		CO	
	E_{ads}	$E_{ads} - E_{ads}^{vdW}$	E_{ads}	$E_{ads} - E_{ads}^{vdW}$	E_{ads}	$E_{ads} - E_{ads}^{vdW}$
$ZrO_2(111)$	--	--	-0.24	-0.01	-0.37	-0.24
$Ni/ZrO_2(111)$	-1.39	-1.21	-1.35	-1.09	-2.70	-2.54
YSZ(111)	-0.82	-0.68	-0.36	-0.15	-0.37	-0.24
Ni/YSZ(111)	-0.67	-0.52	-0.31	-0.09	-2.32	-2.14

when the molecules adsorb weakly onto the surface, the shift in the wavenumber of the stretching mode is negligible and the molecule-surface interaction is mainly due to van der Waals interactions. In Table 3 we compare E_{ads} with ($E_{ads} - E_{ads}^{vdW}$), where E_{ads} and E_{ads}^{vdW} correspond to the total and Van der Waals adsorption energies, respectively. We observe from Table 3 that for the weak adsorptions, such as CO_2-ZrO_2(111) and CO_2-Ni/YSZ(111), ($E_{ads} - E_{ads}^{vdW}$) is approximately equal to zero, indicating that the molecule-surface interaction arises mainly from the Van der Waals interactions. For other systems, such as H_2O-Ni/YSZ(111), CO_2-YSZ(111) and CO-ZrO_2(111), the contribution of the Van der Waals interactions is still non-negligible since ($E_{ads} - E_{ads}^{vdW}$) is approximately twice as high as E_{ads}.

For the strong interactions (H_2O-Ni/ZrO_2(111), CO_2-Ni/ZrO_2(111), CO-Ni/ZrO_2(111) and CO-Ni/YSZ(111)), the shift of the stretching mode is considerable (Fig. 8) and the contribution of the Van der Waals interactions is negligible, since the negative value of ($E_{ads} - E_{ads}^{vdW}$) is lower than −1 eV (Table 3).

4. Conclusion

We have studied systematically the interaction of H_2O, CO_2 and CO on the naked and Ni-decorated ZrO_2(111) and YSZ(111) surfaces, where we have employed DFT with long-range interaction corrections to characterize the bonding character of these molecule-metal-support interfaces. We found that thermodynamically H_2O adsorbs dissociatively on ZrO_2(111), but in the presence of Ni both dissociated and molecular H_2O can coexist. On the other hand, molecular water is likely to be present on YSZ(111) and Ni/YSZ(111), depending on the experimental conditions. Regardless of which surface is considered, the charge transfer is negligible upon H_2O adsorption, except for the dissociated state. CO_2 shows very weak adsorption on the surfaces studied with the exception of Ni/ZrO_2(111), where the molecule is activated by the transfer of 0.5 e^-. Here, the metal is slightly more oxidized leading to a decrease in the stretching modes of CO_2. The CO adsorption depends strongly on the presence of Ni at the surface; On the Ni-decorated surfaces, CO adsorbs more strongly than H_2O and CO_2, while on the naked surfaces CO binds mainly by long-distance interactions. The interatomic distance analysis agrees with the trend in adsorption energies, since on Ni-decorated surfaces the CO-surface distance is smaller than both H_2O-surface and CO_2-surface distances. Thus, it appears that the role of Ni at the TPB is to provide electrons to CO with a subsequent shift in the IR spectrum. We have also explored the relationship between the binding energy and the variation in the stretching modes where we noted a negligible shift in the wavenumber of the stretching mode for the molecules interacting weakly with the surface.

Clearly, the incorporation of a single nickel atom is an approximate model for the triple-phase boundary, and our results may change if the metal-oxide systems were to include finite nickel clusters or even nanoparticles. In future work, we will therefore investigate how Ni clusters of increasing sizes affect the structure and properties of the interface with the zirconia materials, and if the size of the cluster will affect the interaction of the metal clusters with the gaseous molecules.

Acknowledgment

We acknowledge the Engineering and Physical Sciences Research Council (Grant nos. EP/K001329 and EP/K016288) for funding. ACE acknowledges the UCL Doctoral Training Centre in Molecular Modelling and Materials Science (EPSRC grant no. EP/G036675) for a studentship and NHdL acknowledges the Royal Society for an Industry Fellowship.

Via our membership of the UK's HPC Materials Chemistry Consortium, which is funded by EPSRC (EP/L000202), this work made use of the facilities of ARCHER, the UK's national high-performance computing service, which is funded by the Office of Science and Technology through EPSRC's High End Computing Programme. The authors also acknowledge the use of the UCL@Legion High Performance Computing Facility, and associated support services, in the completion of this work. Finally, the authors acknowledge the use of the IRIDIS High Performance Computing Facility, and associated support services at the University of Southampton, in the completion of this work.

Appendix A. Supplementary data

Supplementary data to this article can be found online at http://dx.doi.org/10.1016/j.susc.2016.06.008.

References

[1] P.I. Cowin, C.T.G. Petit, R. Lan, J.T.S. Irvine, S. Tao, Adv. Energy Mater. 1 (2011) 314.
[2] M.C. Muñoz, S. Gallego, J.I. Beltrán, J. Cerdá, Surf. Sci. Rep. 61 (2006) 303.
[3] M.H. Weng, H.-T. Chen, Y.-C. Wang, S.-P. Ju, J.-G. Chang, M.C. Lin, Langmuir 28 (2012) 5596.
[4] S. Kim, H. Moon, S. Hyun, J. Moon, J. Kim, H. Lee, Solid State Ionics 178 (2007) 1304.
[5] S. Kim, H. Moon, S. Hyun, J. Moon, J. Kim, H. Lee, Performance and durability of Ni-coated YSZ anodes for intermediate temperature solid oxide fuel cells, 177 (2006) 931.
[6] J. Hanna, W.Y. Lee, Y. Shi, A.F. Ghoniem, Prog. Energy Combust. Sci. 40 (2014) 74.
[7] A.M. Sukeshini, B. Habibzadeh, B.P. Becker, C.A. Stoltz, B.W. Eichhorn, G.S. Jackson, J. Electrochem. Soc. 153 (2006) A705.
[8] A. Atkinson, S. Barnett, R.J. Gorte, J.T.S. Irvine, A.J. McEvoy, M. Mogensen, S.C. Singhal, J. Vohs, Nat. Mater. 3 (2004) 17.
[9] G.O. Lauvstad, R. Tunold, S. Sunde, J. Electrochem. Soc. 149 (2002) E497.
[10] B. Novosel, M. Avsec, J. Macek, Mater. Technol. 42 (2008) 51.
[11] Y. Matsuzaki, I. Yasuda, J. Electrochem. Soc. 147 (2000) 1630.
[12] L. Andreassi, C. Toro, S. Ubertini, J. Fuel Cell Sci. Technol. 6 (2009) 021307.
[13] A. Hauch, J.R. Bowen, L.T. Kuhn, M. Mogensen, Electrochem. Solid-State Lett. 11 (2008) B38.
[14] Y. Liu, C. Jiao, Solid State Ionics 176 (2005) 435.
[15] K.V. Jensen, S. Primdahl, I. Chorkendorff, M. Mogensen, Solid State Ionics 144 (2001) 197.
[16] X. Xia, R. Oldman, R. Catlow, Chem. Mater. 21 (2009) 3576.
[17] S.P.S. Badwal, Solid State Ionics 52 (1992) 23.
[18] J.E.P.-H.P. Li, W. Chen, Phys. Rev. B 48 (1993) 1063.
[19] L.M. Catlow, C.R.A. Chadwick, A.V. Greaves, G.N. Moroney, J. Am. Ceram. Soc. 69 (1986) 272.
[20] D. Komyoji, A. Yoshiasa, T. Moriga, S. Emura, F. Kanamaru, K. Koto, Solid State Ionics 50 (1992) 291.
[21] G. Stapper, M. Bernasconi, N. Nicoloso, M. Parrinello, Phys. Rev. B 59 (1999) 797.
[22] A. Cadi-Essadek, A. Roldan, N.H. de Leeuw, J. Phys. Chem. C 119 (2015) 6581.
[23] M. Shishkin, T. Ziegler, J. Phys. Chem. C 114 (2010) 11209.
[24] C. Cucinotta, M. Bernasconi, M. Parrinello, Phys. Rev. Lett. 107 (2011) 206103.
[25] S.C. Ammal, A. Heyden, J. Phys. Chem. Lett. 3 (2012) 2767.
[26] M. Shishkin, T. Ziegler, J. Phys. Chem. C 113 (2009) 21667.
[27] G. Kresse, J. Furthmüller, Phys. Rev. B - Condens. Matter Mater. Phys. 54 (1996) 11169.
[28] G. Kresse, J. Furthmüller, Comput. Mater. Sci. 6 (1996) 15.
[29] G. Kresse, J. Hafner, Phys. Rev. B 48 (1993) 13115.
[30] G. Kresse, J. Hafner, J. Phys. Condens. Matter 6 (1994) 8245.
[31] P. Hohenberg, W. Kohn, Phys. Rev. 136 (1964) B864.
[32] J.P. Perdew, K. Burke, M. Ernzerhof, Phys. Rev. Lett. 77 (1996) 3865.
[33] S. Grimme, J. Comput. Chem. 27 (2006) 1787.
[34] P.E. Blöchl, Phys. Rev. B 50 (1994) 17953.
[35] R. Grau-crespo, N.C. Hernandez, J.F. Sanz, N.H. de Leeuw, J. Phys. Chem. C 2 (2007) 10448.
[36] K.R. Hahn, A.P. Seitsonen, M. Iannuzzi, J. Hutter, ChemCatChem 7 (2015) 625.
[37] R.F.W. Bader, Chem. Rev. 91 (1991) 893.
[38] A.D. Becke, K.E. Edgecombe, J. Chem. Phys. 92 (1990) 5397.
[39] S.T. Korhonen, M. Calatayud, A.O.I. Krause, J. Phys. Chem. C 112 (2008) 6469.
[40] V. Hornebecq, C. Kn, P. Boulet, B. Kuchta, P.L. Llewellyn, J. Phys. Chem. C 115 (2011) 10097.
[41] E.J. Walter, S.P. Lewis, A.M. Rappe, Surf. Sci. 495 (2001) 44.
[42] L.G.V. Briquet, C.R.A. Catlow, S.A. French, J. Phys. Chem. C 114 (2010) 22155.
[43] L.M. Molina, M.D. Rasmussen, B. Hammer, J. Chem. Phys. 120 (2004) 7673.
[44] Y. Chen, P. Crawford, P. Hu, Catal. Lett. 119 (2007) 21.
[45] Z. Duan, G. Henkelman, ACS Catal. 5 (2015) 1589.
[46] J. Li, E. Croiset, L. Ricardez-sandoval, J. Phys. Chem. C 117 (2013) 16907.
[47] J. Carrasco, L. Barrio, P. Liu, J.A. Rodriguez, M. Vero, J. Phys. Chem. C 2 (2013) 8241.
[48] V. Yurkiv, A. Gorski, W.G. Bessler, H.-R. Volpp, Chem. Phys. Lett. 543 (2012) 213.
[49] M.A. Henderson, Surf. Sci. Rep. 46 (2002) 1.
[50] H.-J. Freund, M.W. Roberts, Surf. Sci. Rep. 25 (1996) 225.
[51] J. Shimanouchi, "Molecular vibrational frequencies" in NIST Chemistry WebBook, NIST Standard Reference Database Number 69, Eds. P.J. Linstrom and W.G. Mallard, National Institute of Standards and Technology, Gaithersburg MD, 20899, http://webbook.nist.gov., Http://webbook.nist.gov, (Accessed August 2015). (n.d.).
[52] I. Coblentz Society, "Evaluated Infrared Reference Spectra" in NIST Chemistry WebBook, NIST Standard Reference Database Number 69, Eds. P.J. Linstrom and W.G. Mallard, National Institute of Standards and Technology, Gaithersburg MD, 20899, http://webbook.nist.gov., http://webbook.nist.gov, (accessed August 2015). (n.d.).
[53] O. Dulaurent, D. Bianchi, Appl. Catal. A Gen. 207 (2001) 211.
[54] E.-M. Köck, M. Kogler, T. Bielz, B. Klötzer, S. Penner, J. Phys. Chem. C 117 (2013) 17666.